Petroleum Science 21 (2024) 2023–2036

Contents lists available at ScienceDirect

Petroleum Science

journal homepage: www.keaipublishing.com/en/journals/petroleum-science

Original Paper

Mechanical characteristics and reservoir stimulation mechanisms of the Gulong shale oil reservoirs, the northern Songliao Basin

Si-Wei Meng [a, b], Jia-Ping Tao [a, b], Tian-Jiao Li [c], Dong-Xu Li [d], Su-Ling Wang [e], Liu Yang [f], Xin Liu [b, c], Li-Hao Liang [a, b], He Liu [a, b, *]

[a] PetroChina Research Institute of Petroleum Exploration Development, Beijing, 100083, China
[b] National Key Laboratory of Continental Shale Oil, Daqing 163002, Heilongjiang, China
[c] Dalian University of Technology, Dalian, 116024, Liaoning, China
[d] PetroChina Daqing Oilfield Co. Ltd., Daqing, 163002, Heilongjiang, China
[e] Northeast Petroleum University, Daqing, 163002, Heilongjiang, China
[f] China University of Mining and Technology (Beijing), Beijing, 100083, China

ARTICLE INFO

Article history:
Received 25 November 2022
Received in revised form
30 August 2023
Accepted 1 November 2023
Available online 2 November 2023

Edited by Jia-Jia Fei and Min Li

Keywords:
Shale oil
Hydraulic fracturing
High bedding density
Fracture propagation model

ABSTRACT

Shale oil of the Qingshankou Formation of the Gulong Sag, the northern Songliao Basin, represents the first attempt at large-scale development of pure-shale-type shale oil in China. By integrating the multi-scale refined reservoir characterization with macro-micro-scale mechanical testing, it is clarified that the Gulong shale is characterized by high clay mineral content, high rock plasticity, highly-developed bedding, and prominent mechanical anisotropy. A three-dimensional (3D) fracture propagation model of hydraulic fracturing was built for the Gulong shale, which fully captures the hydraulic fracture distribution pattern affected by the high bedding density, in-situ stress, and fracturing treatment parameters. Our research showed that due to influences of bedding, hydraulic fracturing in the Gulong shale forms a complex fracture morphology featuring the main fracture with multiple perpendicular branches that have different lengths (like the outdoor directional TV antenna); however, the vertical propagation of fractures is inhibited, and the fracture height is commonly less than 10 m. The limited stimulated reservoir volume (SRV) is the main problem facing the fracturing stimulation of the Gulong shale oil. Bedding density has vital effects on fracture morphology, so case-specific fracturing designs shall be developed for shale intervals with different bedding development degrees. For reservoirs with well-developed bedding, it is suggested to properly increase the perforation cluster spacing and raise the volume and proportions of viscous fluids of the pad, so as to effectively promote vertical fracture propagation and improve reservoir stimulation performance. This study integrates multi-scale fine reservoir characterization and macro-micro-scale mechanical testing, as well as the construction and numerical simulation of hydraulic fracturing models for high-density layered shale reservoirs, providing a new approach and methodological framework for the fracturing research of high-density layered shale reservoirs.

1. Introduction

China has abundant shale oil, which is an important strategic alternative to conventional petroleum resources (Zhao et al., 2020; Kuang et al., 2022). By far, strategic breakthroughs have been made in key basins, such as the Junggar, Ordos, Bohai Bay, and Qaidam Basins, and good development performance has been delivered in tight sweet-spot oil-enriched thin interlayers of some shale series (Liu et al., 2020). However, with the gradual scale-up of shale oil exploration and development, the proportions of high-quality reserves decline, and trapped oil in shale source rocks inevitably becomes the main target of exploration and development (Jin et al., 2021). The Gulong shale oil in the northern Songliao Basin is the first attempt at large-scale exploration and development of shale oil of the pure-shale type in China. The shale thickness accounts for

* Corresponding author. PetroChina Research Institute of Petroleum Exploration Development, Beijing, 100083, China.
E-mail address: liuhe@petrochina.com.cn (H. Liu).

https://doi.org/10.1016/j.petsci.2023.11.002

more than 90% of the total thickness of the target layer. Well Guyeyouping-1 targeted the pure shale in the lower part of the first Member of the Qingshankou Formation (Qing-1 Member) and delivered high-rate industrial oil streams, revealing tremendous resource potential. However, it is still difficult to reach the threshold of economic production (Sun et al., 2021), and how to cost-effectively deliver the large-scale development of such shale reservoirs is a key problem urgently demanding solutions.

Large complex fracture networks formed via the multi-stage multi-cluster fracturing of horizontal wells are vital to the effective development of shale oil (Nandlal and Weijermars, 2022; Lu et al., 2020; Dong et al., 2021; Zhao et al., 2022). Unlike conventional oil and gas reservoirs and marine-origin shale gas reservoirs that have been commercially developed, the Gulong shale of continental sedimentary origin is characterized by high clay mineral content, high reservoir rock plasticity, and high heterogeneity. The fine core description showed that the Gulong shale has extremely-developed horizontal bedding seams of both organic and inorganic origins, with densities of about several hundred to thousand fractures per meter. Such fractures have critical effects on hydraulic fracture propagation (Sun et al., 2022). When hydraulic fractures meet bedding planes, they have different possible behaviors, such as penetration, deflection, arrest, or step-like extension. This results in high uncertainty of the ultimate fracture network morphology (Zhao et al., 2021; Liu et al., 2023). Therefore, it is of great significance for the optimization of the fracturing treatment parameters of the Gulong shale oil to clarify the mechanical characteristics of the Gulong shale under the controls of high clay mineral content and high heterogeneity and identify fracture propagation mechanisms of hydraulic fracturing (Labani and Rezaee, 2015).

In recent years, global researchers have performed a mass of numerical simulations of hydraulic fracture propagation in bedding-developed shale reservoirs. For example, Heng et al. (2019) carried out true triaxial hydraulic fracturing physical simulations and two-dimensional (2D) numerical simulations to investigate the non-planar growth behavior and evolution process of hydraulic fractures of horizontal wells in shale with bedding planes and reveal the mechanisms of hydraulic fractures penetrating or being arrested/deflected at bedding planes. Chang et al. (2015) developed a numerical model composed of both soft and hard layers and their interfaces to study the fracture propagating behavior at the interface of layered rocks. The simulation results showed that the bedding plane spacing, hard layer thickness, and tensile strength all affect the fracturing mode. Ouchi et al. (2017) systematically researched the control mechanisms of bedding mechanical properties, dip angles, interface characteristics, and in-situ stress differences on the propagation dynamics of hydraulic fractures, using a fully three-dimensional (3D) poroelastic geological model with undefined crack propagation paths. With a flow-stress-damage-coupled (FSD-coupled) numerical model, Wang et al. (2016) probed into the effects of various uncertain factors, including the in-situ stress, bedding plane density, rock brittleness, fracture toughness, injection rate, and fluid viscosity on hydraulic fracture propagation behaviors and stimulated reservoir volumes (SRVs) via a response surface method. Using a discrete element approach, Zhou et al. (2020) built a 3D fracture propagation model of shale incorporating mechanical anisotropy, bedding seams, and in-situ stress differences to analyze the hydraulic fracture distribution patterns in cases of different densities and strengths of bedding and diversified fracturing treatment parameters. However, few previous studies have studied hydraulic fracturing simulations of reservoir shales at the mine scale and considered dense laminar distribution to simulate the process of hydraulic fracture sprouting and expansion. The construction of hydraulic fracturing research model and the assignment of numerical simulation parameters, especially the assignment of mechanical parameters of bedding, are highly subjective and lack of strong evidence.

The models of the above numerical simulation studies incorporate bedding of shale-specifically, influences of shale bedding on hydraulic fracture propagation behaviors. However, the bedding density of these models, at most, reaches only the meter scale, which fails to meet the simulation requirements of the Gulong shale with high-bedding-seam-density. Hence, this research targeted the Gulong shale in the Songliao Basin, systematically described the material-structural dual heterogeneity of the shale layers, and clarified the influences of such heterogeneity on mechanical properties. Then, based on the mechanical characterization of shale, a model of high-bedding-density shale was established, which fully couples the fluid flow and damage evolution and propagation of elements. Furthermore, a 3D fracture propagation model of hydraulic fracturing considering the high bedding density of shale was built for the finely-laminated Gulong shale oil, and the hydraulic fracture propagation patterns and main control factors of high-bedding-density shale were clarified. The findings of this research provide effective theoretical guidance for fracturing design and treatment optimization of high-bedding-density shale reservoirs.

2. Study area overview and research methodology

2.1. Study area overview

The Songliao Basin is a large continental Mesozoic-Cenozoic sedimentary basin. The deep-water sediments of the Cretaceous Qingshankou Formation in the Gulong Sag of the northern basin provide the material basis for the formation of the framework of the fine-grained sedimentary cycle. The developed dark shale features large thickness, high organic matter abundance, moderate thermal maturity, and high oil generation capacity, which are beneficial to the coming-into-being of hydrocarbon accumulations with industrial values in mudstone/shale series.

Three wells were drilled previously, with systemic coring of the Qingshankou Formation. The observation of collected 765-m-long cores showed laminated shale has the highest development, with a single-layer thickness of 30–120 m and the cumulative thickness accounting for about 85% of the total shale thickness. The predominance of felsic, argillaceous, and mixed laminations is observed, with occasional development of pyrite laminations. The mineral composition of different laminations varies from each other, which leads to differentiated mechanical properties. Different laminations are peeled off from each other along their interfaces, and thus high-density weak planes and bedding seams are formed (Feng et al., 2020). As revealed by the fine core description, the shale bedding density of the Qingshankou Formation mostly lies between 780 bedding/m and 2800 bedding/m, and in some local areas, it can exceed 4000 bedding/m (Liu et al., 2018).

2.2. Samples and experimental characterization methods

The samples were collected from the shale of the 1st Member of the Qingshankou Formation of Wells A and B in the Songliao Basin (Fig. 1). For comparison, the shale samples of the Longmaxi Formation of Well C in the Sichuan Basin and those of the Chang 7 Member of the Yanchang Formation of Well D in the Ordos Basin were included. The main experimental methods are summarized below:

(1) The mineral composition was measured using the Rigaku D/max 2500 PC Model X-ray diffractometer (XRD). Samples

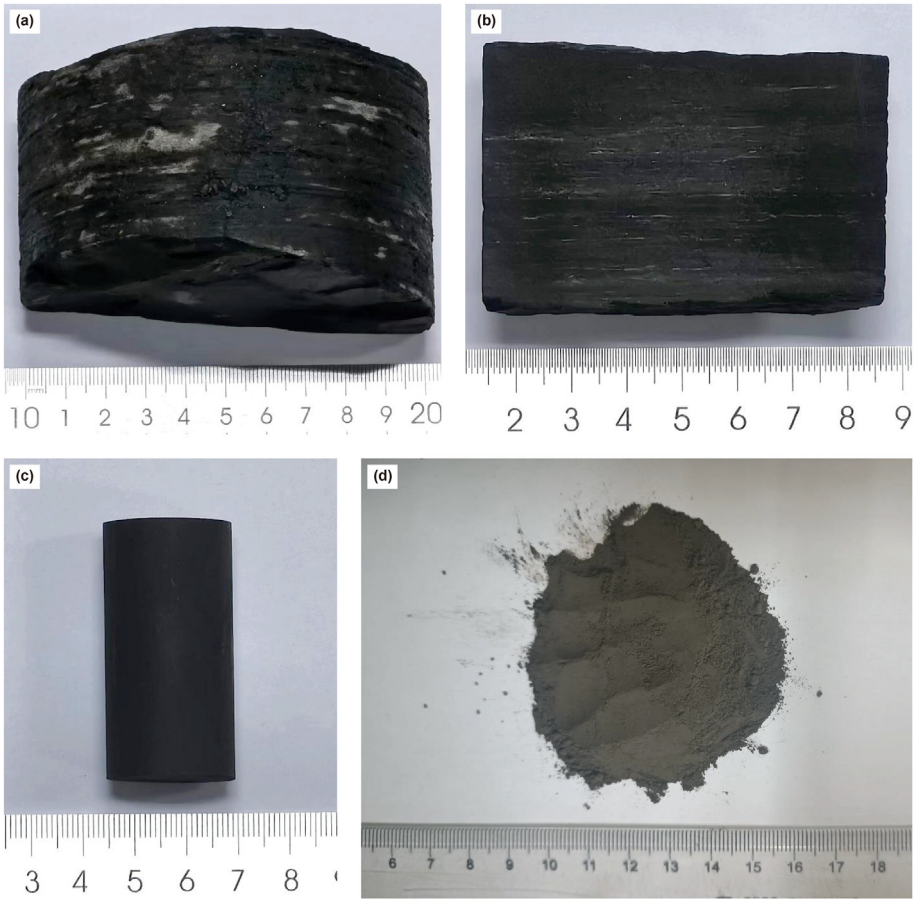

Fig. 1. Gulong shale cores of the 1st Member of the Qingshankou Formation: (**a**) full-diameter samples; (**b**) blocky samples; (**c**) cylindrical samples; (**d**) powder samples.

were ground into powder with particle sizes of 125–150 μm and then placed into the sample disk. The XRD data were acquired at a scanning rate of 1°/min from 3° to 85°, and the mineral composition of samples was determined via the spectrogram analysis.

(2) Large-area elemental scanning was performed using the Bruker M4 TORNADO X-ray fluorescence (XRF) spectrometer. Under the face scan mode, the surface elemental distribution analysis, with resolutions at the centimeter scale, was accomplished by moving the sample stage. The target materials of the X-ray optics of this device were Rh. The working voltage was 50 kV, and the working current was 200 μA. The device can provide the elemental distribution references for the elements between Na and U, with a maximum resolution of up to 20 μm.

(3) The MTS nano-indentation instrument with the Berkovich indenter was used to perform nano-indentation tests. For each sample, 100 points on its surface were tested. The nano-indentation was combined with mineral identification via scanning electron microscopy (SEM) to determine the microscopic mechanical properties of different minerals of the Gulong shale.

(4) The shale scratch test was carried out using the HADHJ-25/100-IV scratch test device to continuously capture the vertical distribution of mechanical properties of shale. The sample dimensions were φ100 mm × 50–500 mm. The cutter width was 2–8 mm, the cutter penetration was 0–1 mm, and the horizontal displacement range was 0–500 mm.

(5) The uniaxial compression tests were performed using the CMT5105 digital universal testing machine. The collected core samples were made into φ25 mm × 50 mm cylinders. The axes of these shale cylinders were either parallel with or perpendicular to bedding. The compression test was performed at a displacement rate of 0.015 mm/min. The stress-strain curves of samples were obtained, and the elastic moduli were computed.

2.3. Three-dimensional fracture propagation model of hydraulic fracturing

To investigate the influences of geological and engineering parameters on hydraulic fracture propagation during hydraulic fracturing of the Gulong shale, the Q2 payzone of the 1st Member of the Qingshankou Formation with depths of 2555.4–2571.4 m was taken as the simulation target, and a numerical model of 180 m × 150 m × 17 m was built in the RFPA3D (percolation analysis version) (Li et al., 2013, 2019). RFPA3D is based on the idea that heterogeneity leads to macro non-linearity and causes progressive failure behavior observed in brittle rock (Li et al., 2019). It is developed with the following assumptions (Li et al., 2019): (1) The properties of each element conform to the Weibull distribution to consider the heterogeneity of the rock mass; (2) An element is treated as an elastobrittle material with a residual strength; (3) Elastic modulus of the element gradually declines with damage, when the element satisfies failure criteria (Eq. (1)); (4) The coupled process between stress/strain and fluid flow in the deforming rock

mass is governed by Biot's consolidation theory (Eq. (2)); (5) The fluid is governed by Darcy's law (Eq. (3)); (6) The hydraulic behavior responds to changes in stress field by permeability variation. However, it is worth noting that the connection between the layers of the unit is a perfect bond, and the phenomenon of displacement inconsistency is not considered.

$$E_d = (1 - D)E_i \tag{1}$$

$$\boldsymbol{\sigma} = 2G\boldsymbol{\varepsilon} + \frac{2\nu G}{1 - 2\nu}\mathrm{tr}(\boldsymbol{\varepsilon})\boldsymbol{I} - \alpha p\boldsymbol{I} \tag{2}$$

$$\frac{\rho g \kappa}{\mu}\nabla^2 H - q = S\frac{\partial H}{\partial t} \tag{3}$$

where E_d is the elastic modulus of a damaged element, Pa; E_i is the initial elastic modulus, Pa; D is the damage variable; $\boldsymbol{\sigma}$ is the stress tensor, Pa; G is the shear modulus, Pa; ν is the Poisson ratio; $\boldsymbol{\varepsilon}$ is the strain tensor; α is the Biot's coefficient; p is the pore pressure, Pa; ρ is the fluid density, kg/m^3; μ is the viscosity, Pa·s; q is the volume source,/s; κ is the permeability, m^2; S is storativity, m^{-1}, $\boldsymbol{I}$ is the unit tensor.

The boundary conditions of the model are presented in Table 1. To mimic the high bedding density of the Gulong shale, the mesh is encrypted in the vertical direction. The mesh size is 1 m in the horizontal direction and 0.25 m in the vertical direction. The randomly-distributed bedding-parallel elliptical slices were placed to represent the high-density bedding. As shown in Fig. 2, the model is composed of three geological materials, representing the payzone, cap rock, and bedding, respectively. The thickness of the payzone is 10 m, and those of the overlying and underlying cap rocks are 4 and 3 m, respectively. The parameters of geological materials are directly determined based on the well logging interpretation and rock mechanics tests (Table 2). As per actual

Table 1
In-situ stress conditions of the numerical model.

Parameters	Symbols	Units	Values
Vertical stress	σ_x/σ_v	MPa	61.6
Maximum horizontal principal stress	σ_y/σ_h	MPa	47.7
Minimum horizontal principal stress	σ_z/σ_h	MPa	46.2
Initial formation pressure	P_{p0}	MPa	44.3

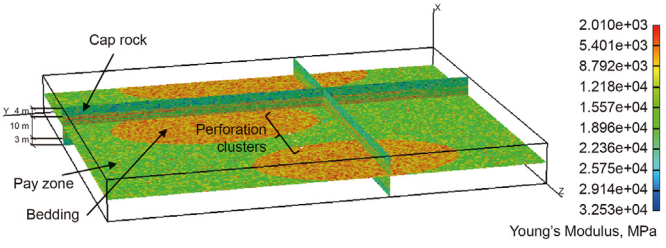

Fig. 2. Numerical model built in RFPA3D (percolation analysis version).

Table 3
Variables of the numeral model.

Variables	Units	Values
Number of bedding n	–	100, 200, 300, 400
Cluster spacing dz	m	4, 6, 8, 10, 12
Fracturing fluid viscosity μ	cP	5, 20, 60
Injected fluids Q	m^3	500, 1000, 1500, 2000, 2500

fracturing treatment, 7 perforation clusters were placed in the model and the pump rate of hydraulic fracturing was 14 m^3/min. Four groups of fracture propagation simulations with varying model parameters (Table 3) were performed separately to explore the influences of the bedding density, cluster spacing, injected fracturing fluid volume and fracturing fluid viscosity on hydraulic fracture propagation in shale. The model with 200 beddings, a cluster spacing of 10 m, and a fracturing fluid viscosity of 20 cP was the reference case.

3. Mechanical characteristics of the Gulong shale

3.1. Material heterogeneity and its mechanical response

The results of the XRD analysis of shale of the 1st Member of the Qingshankou Formation in the Songliao Basin are shown in Fig. 3. The mineral composition is complex and predominated by clay minerals and quartz. The content of clay minerals is 23.5%–53.2% (averaging 38.3%) and that of quartz is 13.8%–39.2% (averaging

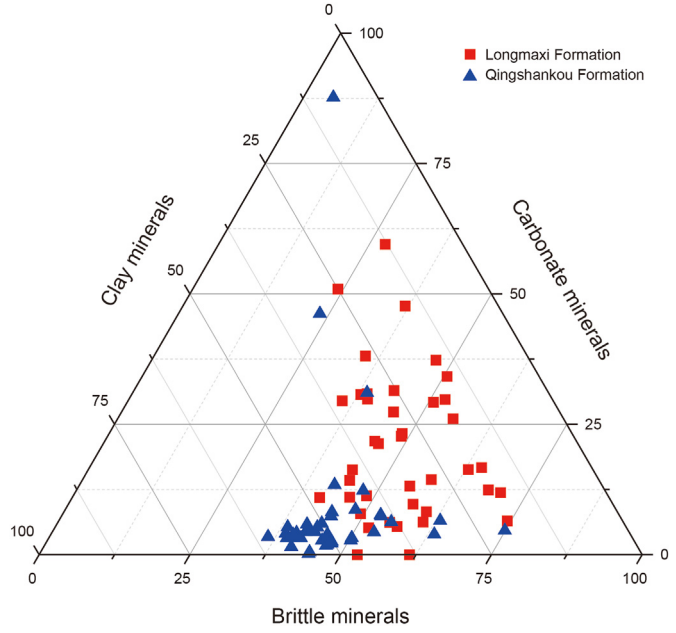

Fig. 3. Comparison of mineral composition between the Qingshankou Formation and Yanchang Formation.

Table 2
Mechanical and fluid flow parameters of the numerical model.

Parameters	Symbols	Units	Payzone	Cap Rock	Bedding
Elastic modulus	E	GPa	14.2	19.3	6.46
Poisson's ratio	ν	–	0.3	0.3	0.3
Uniaxial compressive strength	δ_c	MPa	63	109	34.2
Tensile strength	δ_t	MPa	4.2	5.0	1.6
Permeability	K	m^2	6.2×10^{-19}	6.2×10^{-19}	1×10^{-16}

about 26.9%), followed by the content of feldspar (about 14.5% on average) and carbonate minerals (about 15.5% on average). In comparison, the quartz content of marine-origin shale of the Longmaxi Formation in the Sichuan Basin is 22.1%–69.3% (averaging about 42.1%); the clay mineral content is 12.4%–47.6% (averaging 29.0%); the average carbonate mineral content is about 20.2%; the average feldspar content is extremely low, only 7.5%. Clearly, the Gulong shale has extremely high clay mineral content.

Nano-indentation testing was introduced to calibrate the mechanical properties of the main minerals in the Gulong shale (Oliver and Pharr, 1992; Veytskin et al., 2017; Meng et al., 2021). The obtained SEM images, displacement-load curves, and calculated elastic moduli and hardness are shown in Fig. 4. The micro-mechanical properties of different minerals in the Gulong shale are significantly differentiated. As is made evident by the nano-indentation tests, the displacement-load curves of quartz and feldspar are similar—the dominant elastic deformation, with minor plastic deformation, and the hardness and elastic modulus that are both high. For clay minerals, such as chlorite and illite, the curves are characterized by dominant plastic deformation, low hardness, and small elastic moduli. The mechanical characteristics of dolomite lie between those of brittle and clay minerals. Dolomite presents relatively considerable plastic deformation and yet, is associated with relatively high elastic moduli and hardness.

3.2. Structural heterogeneity and its mechanical response

The Gulong shale has a prominent characteristic—the extremely-developed laminations. Due to differentiated mechanical properties among laminations, the high-bedding-density structure of the Gulong shale is formed. The core sample photo and corresponding elemental scan of the Gulong shale are shown in Fig. 5. The core sample is generally gray-black and black, with no visible hydrocarbon show. The high-frequency interbedding between clay-rich shale laminations and felsic laminations is observed. The elemental scan demonstrates the presence of more than 50 bands with significantly different elemental composition along a 5-cm-long core sample, and the lamination-density is about 1–2 laminations/mm. An abrupt change of elemental composition is found at the interface, which indicates the transition of the clay-rich shale lamination into the felsic lamination, leading to considerable variation of shale mechanical properties.

To clarify the influences of high-density laminations and bedding on mechanical properties, the continuous vertical profile of the Gulong shale mechanical strength was plotted via the scratch test. Moreover, the non-uniform distribution of rock mechanical properties was quantitatively evaluated, and the mechanical weak planes were identified. The calculation formula of compressive strength is as follows:

$$\sigma = \frac{F_T}{A(d)} \tag{4}$$

where σ is the compressive strength, MPa; F_T is the lateral force, N; $A(d)$ is the area, mm^2.

The post-test core photo and the measured compressive strength log are shown in Fig. 6(a). Along the scratch trough of the sample clear high-frequency interbedding of thin beds is seen, and

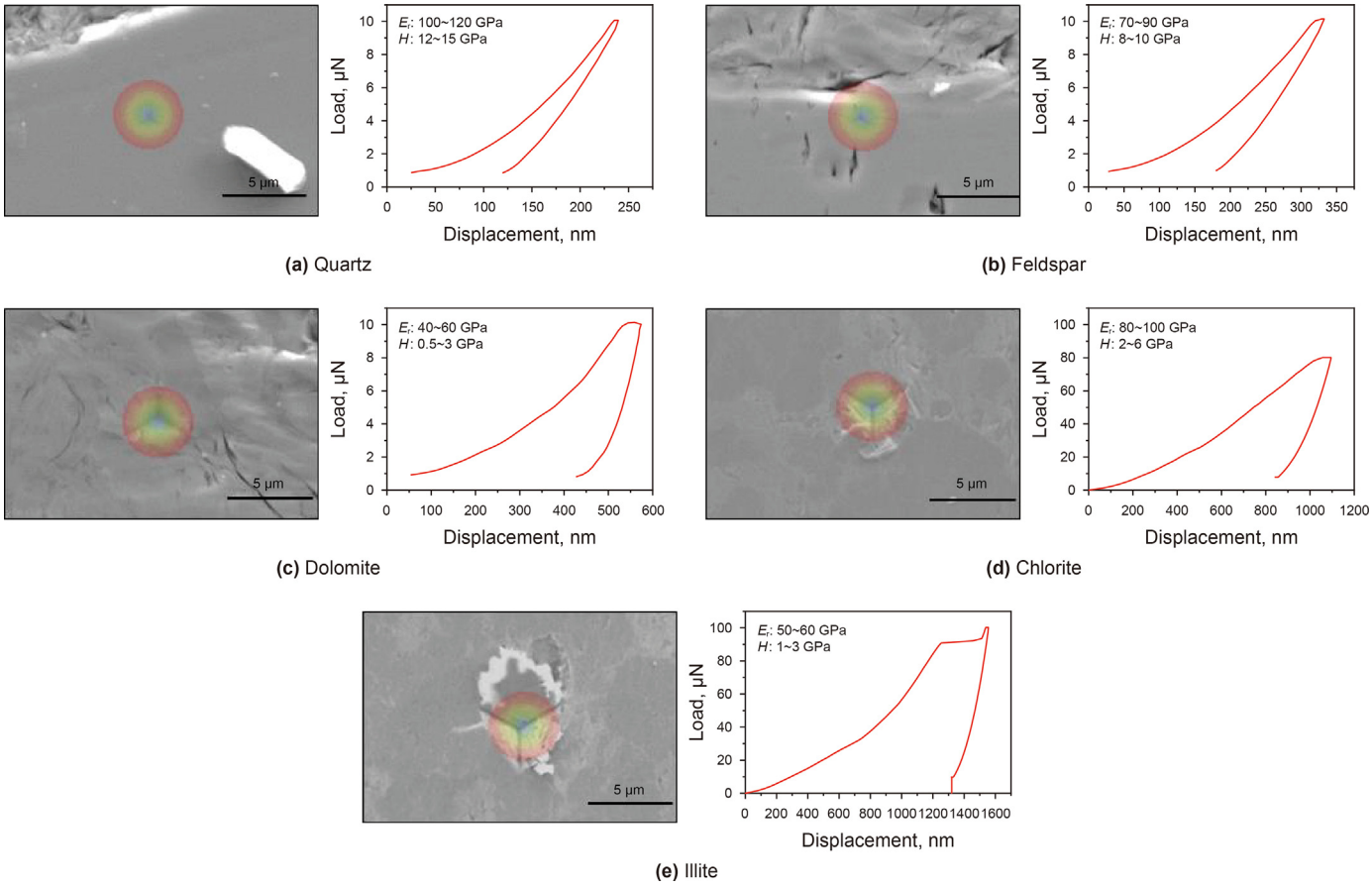

Fig. 4. Nano-indentation results of main minerals in the Gulong shale.

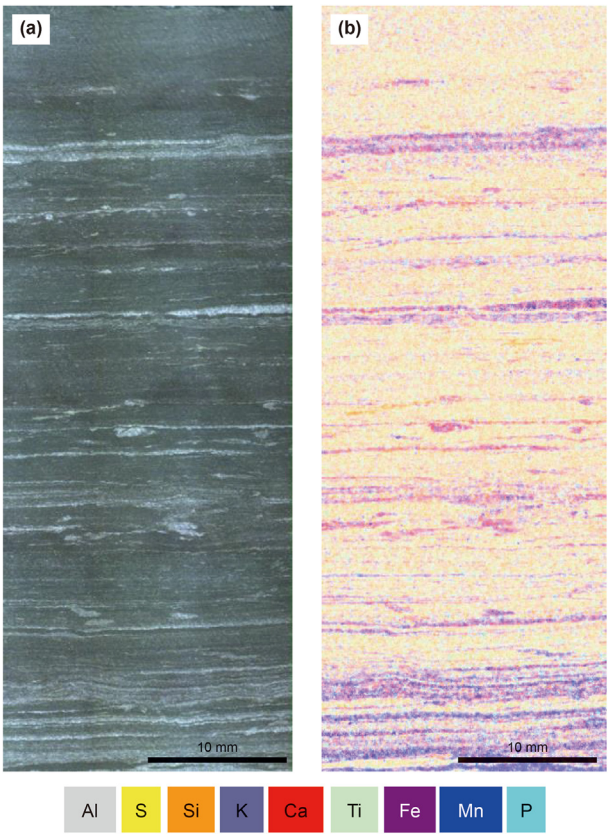

Fig. 5. Large-area scans of a representative Gulong shale sample: (**a**) optical scan and (**b**) elemental scan.

a large number of failure planes occur on both sides of the scratch trough. The compressive strength of the tested sample also presents high-frequency fluctuation. Statistics show 24 fluctuations of compressive strength with amplitudes greater than 18 MPa for the 37-mm scratched section, averaging 6.49 fluctuations/cm and indicating the characteristic of high-frequency interbedding between soft and hard rocks. The shale samples from the Chang 7 Member of the Yanchang Formation in the Ordos Basin were tested for comparison (Fig. 6(b)). Clearly, the Chang 7 Member shale only presents the stratified structure in the middle section, and the failure planes are also concentrated on both sides of the scratch trough of the middle section of the sample. Its compressive strength is comparable to that of the Gulong shale, but the strength fluctuation intensity is greatly reduced. Along the 35-mm tested section, only 7 fluctuations are found with amplitudes greater than 18 MPa, averaging only 2 fluctuations/cm (a reduction by 69.18%, compared with that of the Gulong shale), and such fluctuations are concentrated in the middle of the tested sample. By observing the surface characteristics of the sample corresponding to the compressive strength peak of the millimeter scale scratch curve, softer minerals and microcracks along the scratch path can cause the compressive strength curve peak to decline rapidly within a short displacement. In Fig. 6, the red shear head is used to point to the softer minerals, and the white arrow is used to point to the location of the microcracks. This corresponds to the peak decrease in the compressive strength curve on the right. The scratch curve in Fig. 6(b) is relatively concentrated in the 35–25 mm scratch range as a whole. After the rock test on the left, it can be observed that the section is flat and smooth, and the mineral mechanical characteristics are uniform. After the indenter passes through the microcracks, the scratch curve fluctuates significantly and peak points appear in succession. This provides a reference for further exploring the effects of microscale mineral properties and microcracks on mechanical characteristics.

3.3. Transversely isotropic mechanical properties of the gulong shale

Shale is a stratified sedimentary rock, and its mechanical properties are often different in the directions parallel and perpendicular to the bedding. Therefore, shale is anisotropic-specifically, transversely isotropic. Shale with different bedding densities is associated with varied strengths. To characterize the transverse isotropy of shale with different bedding densities, the anisotropic elastic modulus was introduced:

$$\lambda_E = \frac{E_h}{E_v} \tag{5}$$

where E_h is the elastic modulus parallel to the bedding direction; E_v is the elastic modulus perpendicular to the bedding.

The uniaxial compression tests of the Gulong shale were performed to measure the transversely isotropic mechanical parameters (Fig. 7). The bedding-parallel elastic modulus is 16.2 GPa, while that perpendicular to bedding is only 8.48 GPa. The anisotropy ratio reaches 1.91. The main reason is that when the stress is loaded in the normal direction of bedding seams, the inter-lamination compaction and closure of bedding seams lead to an increase in axial strains and therefore, a significant decrease of the elastic modulus perpendicular to bedding.

The shale in the Sichuan Basin, with the burial depth similar to that of the Gulong shale (Wang et al., 2017), was used to comparatively investigate the strength anisotropy of the Gulong shale under the control of high bedding density (Table 4). The bedding-parallel and bedding-perpendicular elastic moduli of the Sichuan shale are 23.25 and 19.92 GPa, respectively, and the anisotropy ratio is only 1.17, which suggests the mechanical properties of the Sichuan shale are also transversely isotropic. However, such Sichuan shale is of marine deposition (Zou et al., 2016). Compared with the Gulong shale of the continental deposition in the Songliao Basin, the rock heterogeneity of the Sichuan shale is relatively lower, and the bedding development is suppressed, due to the more stable marine sedimentary environment. This leads to a significant decrease in the elastic modulus anisotropy. Meanwhile, the elastic modulus of the Gulong shale is greatly lower than that of the Sichuan shale. As stated in Section 3.1, this is mainly attributed to the high content of clay minerals (such as chlorite and illite), resulting in the generally high plasticity of the Gulong shale reservoir rock.

4. Simulation results and analysis

As stated above, the Gulong shale oil reservoir is characterized by a high content of plastic clay minerals, prominent bedding structure and high vertical heterogeneity of mechanical property distribution. Hence, its fracture propagation mechanism is considerably different from that of conventional reservoirs and marine-origin shale gas reservoirs that have achieved large-scale commercial development. Zhang et al. (2020) reported that the Gulong shale in the Songliao Basin is significantly from shale in other basins in the world. Their fracturing monitoring results showed that the hydraulic fractures of the Gulong shale have a large horizontal extension and yet, limited vertical propagation—the fracture height is generally less than 10 m, which severely restrains the SRV. For the recovery of the Gulong shale oil, how to optimize

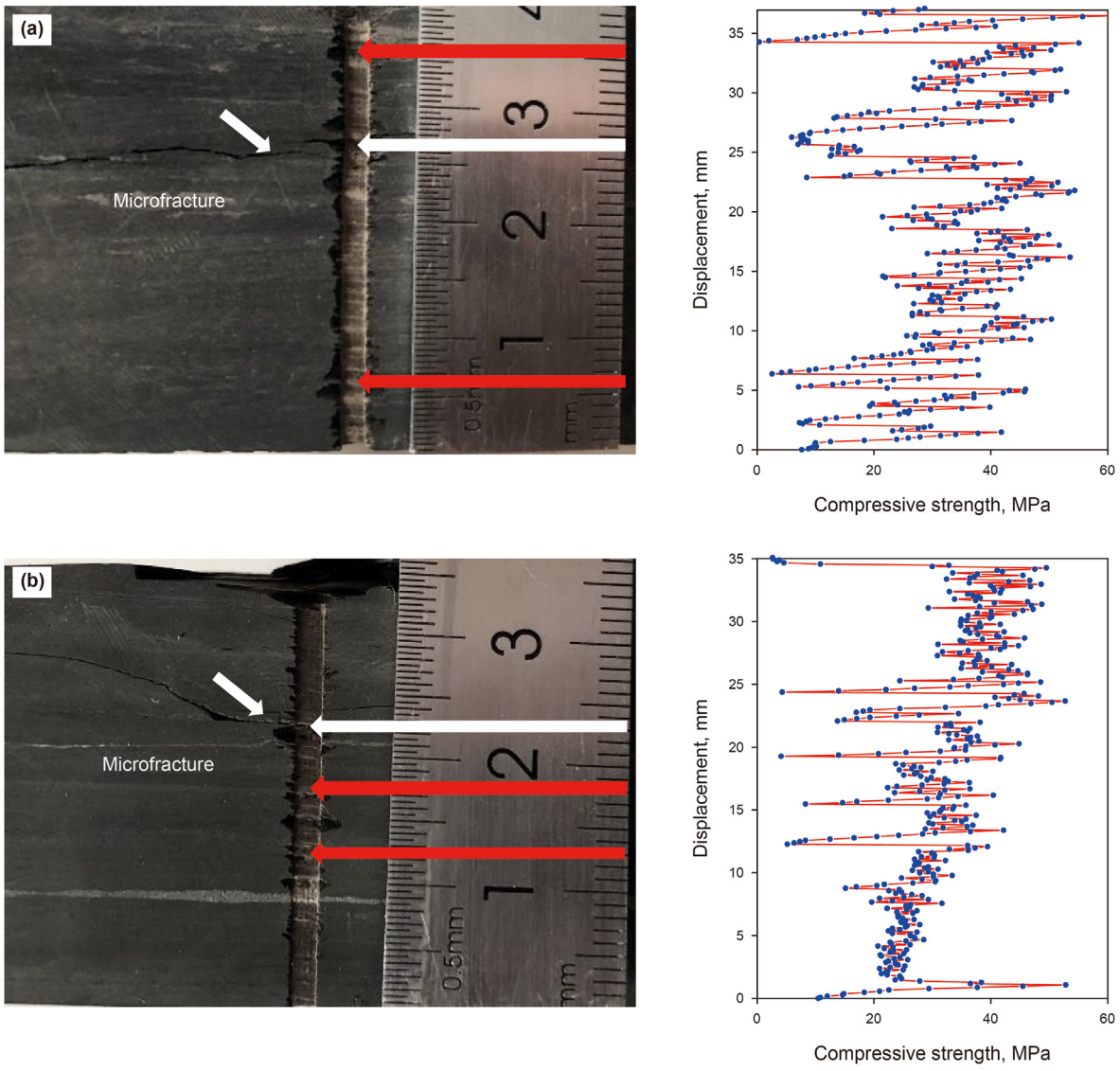

Fig. 6. Shale samples and continuous distribution of compressive strength: (**a**) the Gulong shale, (**b**) the Yanchang Formation shale.

the hydraulic fracturing technology and treatment parameters to improve the performance of reservoir stimulation is an urgent problem to deal with. Based on the 3D fracture propagation model of the high-bedding-density Gulong shale, the hydraulic fracture propagation patterns of high-bedding-density shale were investigated. Moreover, the main geological and engineering factors affecting fracturing performance were identified, to provide theoretical guidance for optimizing fracturing treatment parameters.

(1) Dynamic propagation process of hydraulic fractures

Fig. 8 illustrates the hydraulic fracture propagation process of the slice at y = 87 m of the reference case (bedding quantity = 200, cluster spacing = 10 m and fracturing fluid viscosity = 20 cP). At the beginning of fracturing, the fracture propagates mainly along the direction perpendicular to the minimum horizontal principal stress, and the propagation speeds are similar along the fracture height and length. Then, the fracture encounters the weak horizontal bedding plane during its vertical extension, and the weak plane fails immediately, to form a T-shaped fracture. The main fracture branches at the weak plane or is deflected to propagate along the bedding. The length and aperture of the T-shaped fracture increase until it meets the matrix. The matrix stress gradually builds up, which leads to failure of the matrix and variation of the "T"-shaped structure. The main fracture continues to extend in the matrix ahead and gradually approaches the next weak plane. The above process is repeated and finally, a complex fracture network composed of the main fracture and several branch fractures that have varied lengths and are perpendicular to the main fracture (resembling the bar-type outdoor directional TV antenna) is formed. Due to the anisotropy of materials and the random distribution of bedding, the stress accumulated in each step of fracture propagation is different, and the lengths of perpendicular fracture branches are varied. Fig. 9 shows the observed interaction behavior between propagating hydraulic fracture and pre-existing laminations in some typical slices. The interaction behavior can be summarized into several types: deflect, arrest, branch, connect, cross, bypass, and active. The high-density bedding is considered a "double-edged sword" for the Gulong shale reservoir stimulation. Although it improves the fracture complexity of fractures, it does suppress the vertical propagation of fractures. The simulation showed that the fracture heights of the seven perforation clusters

Fig. 7. Uniaxial compression tests of the Gulong shale.

Table 4
Comparison of characteristic elastic parameters for shale anisotropy.

No.	Sources	Burial Depths, m	E_h, GPa	E_v, GPa	λ_E
1	Gulong shale, Daqing	2000–2500	16.20	8.48	1.91
2	Sichuan shale	2312–2319	23.25	19.92	1.17

are all less than 10 m. How to promote the vertical layer penetration of hydraulic fractures and increase the fracture height is a great challenge of hydraulic fracturing in the Gulong shale.

(2) Influences of bedding density

To clarify the influences of the bedding density on fracture propagation, the cluster spacing and fracturing fluid viscosity were kept at 10 m and 20 cP, respectively, while the number of bedding was set as 100, 200, 300 and 400 for simulations. The fracture morphologies of the four models with the injected volumes of 2100 m^3 for the slices of $y = 67$ m and $z = 64$ m are shown in Fig. 10. With the increasing bedding quantity, the number of horizontal fractures grows, and so does the fracture network complexity. However, the increasing bedding quantity leads to a large horizontal leak-off of fracturing fluids, and this inhibits the height propagation of the main fracture. Therefore, bedding have important influences on the fracture propagation dynamics in the Gulong shale. For shale intervals with the different occurrence of bedding, the fracturing designs shall be performed in a case-specific manner.

Fig. 11 shows the relationship between the accumulated AE event counts of models with different quantities of laminations and the volume of injected fracturing fluid. As can be seen from the figure, compared with the model without laminations, the model

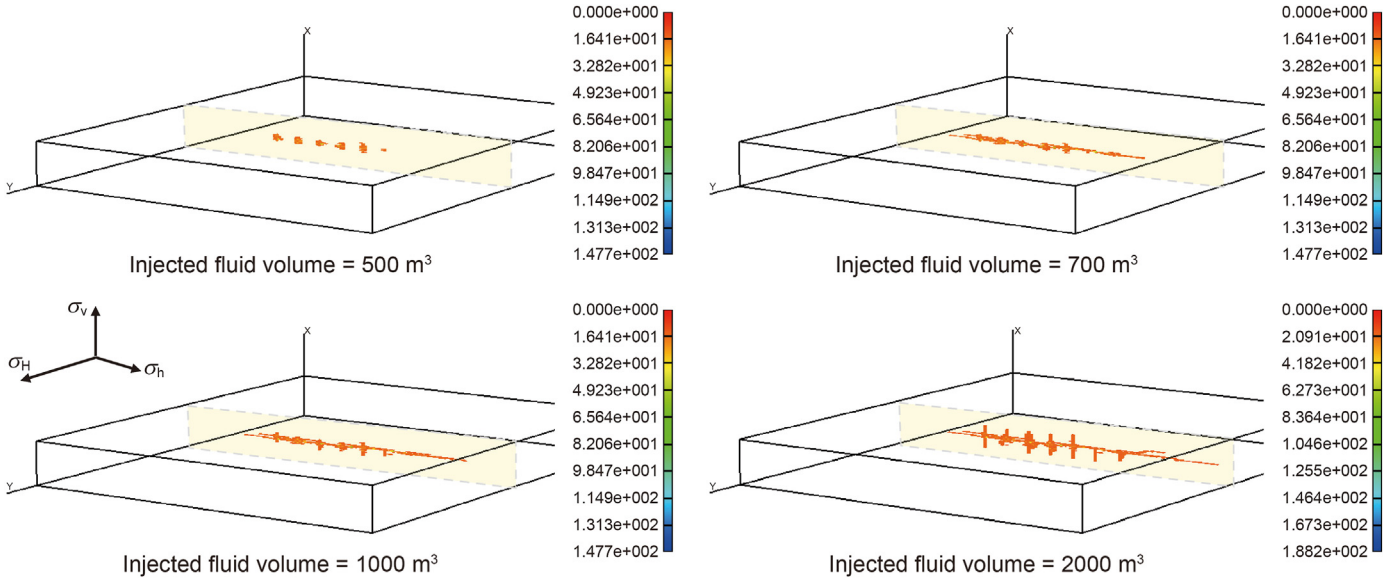

Fig. 8. Fracture width (mm) and fracture morphology vs. injected fluid volume ($y = 87$ m) of the reference case.

with laminations breaks earlier, and the accumulated AE event counts increase significantly. As the number of joints increases, the number of accumulated AE increases. This indicates that the laminations can increase the reconstruction volume due to their high permeability and low strength. At the same time, the intact model has obvious steep sections, which is because when there is no lamination in the model, the breakdown pressure is high, resulting in sudden large-scale rupture.

(3) Influences of cluster spacing

Perforation cluster spacing is an important engineering parameter. In reservoir stimulation of unconventional hydrocarbon resources, smaller clustering spacing is often adopted—by greatly shortening the cluster spacing and raising the fracturing intensity, the migration distance of oil and gas to artificial fractures is reduced, and the well productivity is enhanced (Lu et al., 2022). However, when the cluster spacing is small, the compressive stress between fractures increases during multi-fracture propagation, which may cause uneven fracture propagation between perforation clusters and subsequently impact the fracturing performance (Wang et al., 2018; Ren et al., 2018). Given this, a group of simulations were carried out to evaluate the influences of cluster spacing on the reservoir stimulation performance of the Gulong shale. In such simulations, the model was placed with constant 200 bedding, and the fracturing fluid viscosity was fixed at 20 cP, while the cluster spacing was assigned with 4, 6, 8, 10 and 12 m, respectively. The simulation results of the slice $x = 9$ m were compared and analyzed (Fig. 12). The planar bedding distribution within this slice is shown in Fig. 12(a).

The comparison of Fig. 12(b)–(f) reveals that the morphologies of hydraulic fractures propagating parallel to bedding are similar, in cases of different cluster spacing—they are all found with fracture intersection and propagation deflection of some fractures. This is mainly attributed to the high permeability and low strength of bedding. The high permeability of bedding accelerates the rapid dissipation of water pressure in hydraulic fractures, and the low bedding strength attracts hydraulic fractures to deflect and enter the bedding, or branch at the bedding. Fig. 13 demonstrates the influence of cluster spacing on the fracture length. At the early stage of fracture propagation, wider cluster spacing results in longer fractures. However, at the last stage of fracture propagation, the final fracture length is controlled by beddings. Fig. 14 visualizes the hydraulic fracture propagation from another angle of view. As is

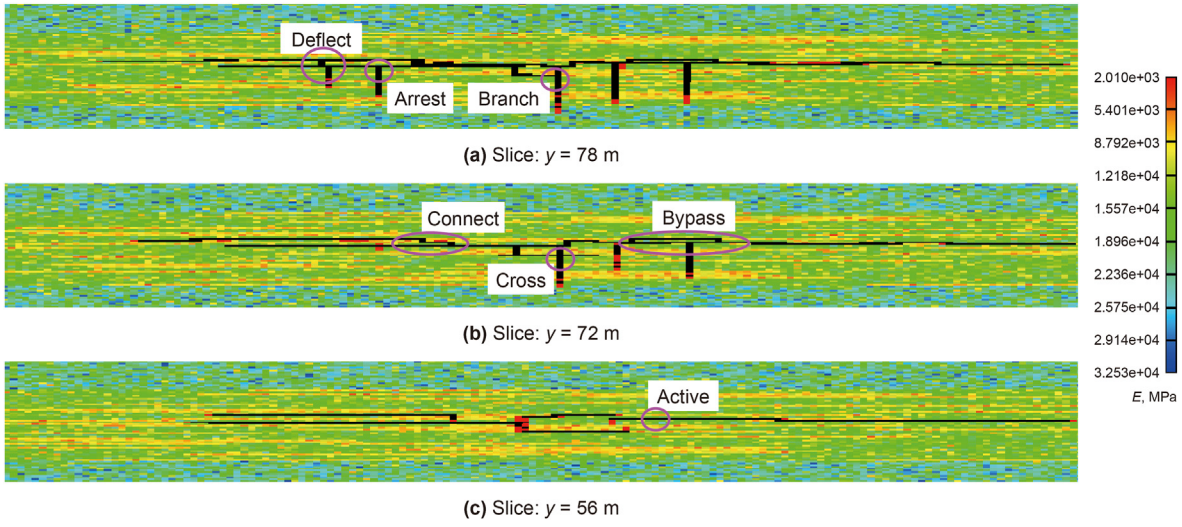

Fig. 9. Observed interaction behavior between propagating hydraulic fracture and pre-existing laminations.

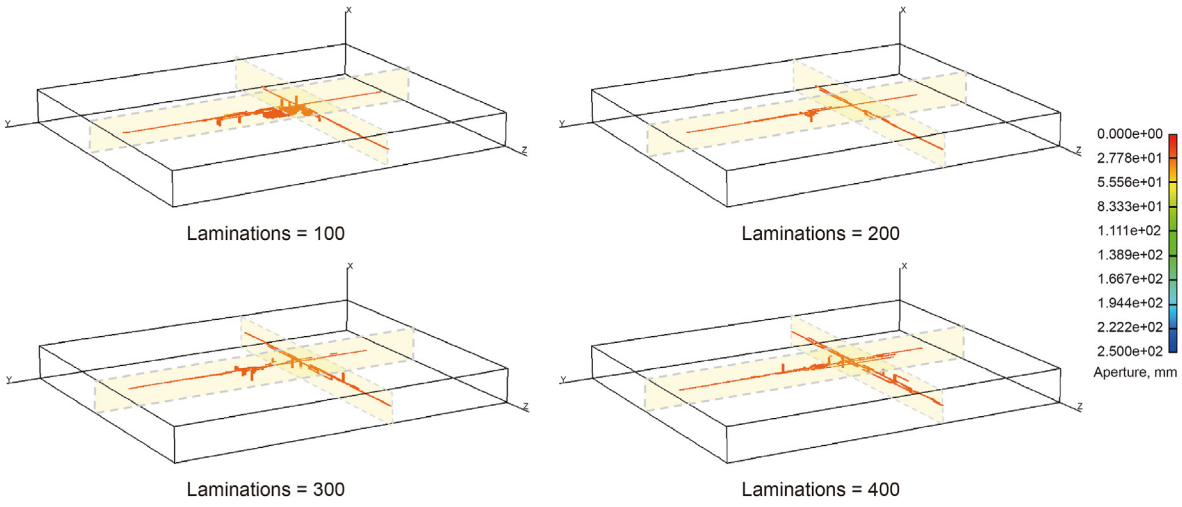

Fig. 10. Fracture distribution of the model slices ($y = 67$ m and $z = 64$ m) with injected fluids of 2100 m^3, in cases of different quantities of laminations.

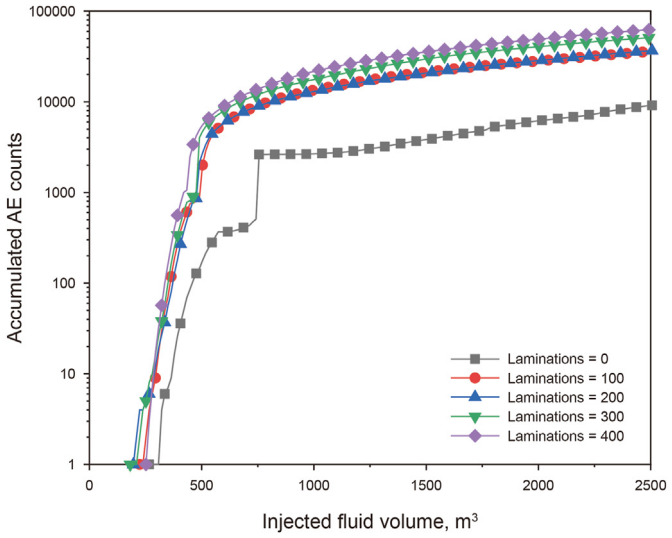

Fig. 11. Influence of quantities of laminations on the accumulated AE event counts.

made evident by Fig. 12(b)–(f), with the cluster spacing less than 10 m, the vertical propagation of hydraulic fractures is inhibited, and only about half of the perforation clusters are effectively propagated. This is mainly because the Gulong shale reservoir has highly developed bedding, and its effective horizontal permeability is much higher than the effective vertical permeability, which aggravates the vertical stress interference between the fractures of each cluster. Given the aforementioned, the reservoir stimulation of the Gulong shale shall not excessively raise the fracturing intensity and shorten the cluster spacing, especially for shale intervals with highly developed bedding (in such intervals, the cluster spacing shall be no less than 10 m).

(4) Influences of treatment scales

The treatment scale refers to the injected fluid volume during the fracturing treatment and is a main engineering parameter to control fracture lengths. The fracture lengths and average fracture widths versus injected fluid volume are plotted for the reference case (bedding quantity = 200, cluster spacing = 10 m and fracturing fluid viscosity = 20 cP) (Fig. 15). With the injected fluid less than 500 m^3, the fracture length and average fracture width both increase rapidly. Then, the average fracture width gradually declines and finally reaches the equilibrium, because of the pressure drop inside the fracture and the neglect of proppants in our models. The fracture length increases gradually with the increasing volume of the injected fluid but the growth rate declines gradually. After 2800 m^3 of fluid are injected, the fracture length reaches 142 m. The

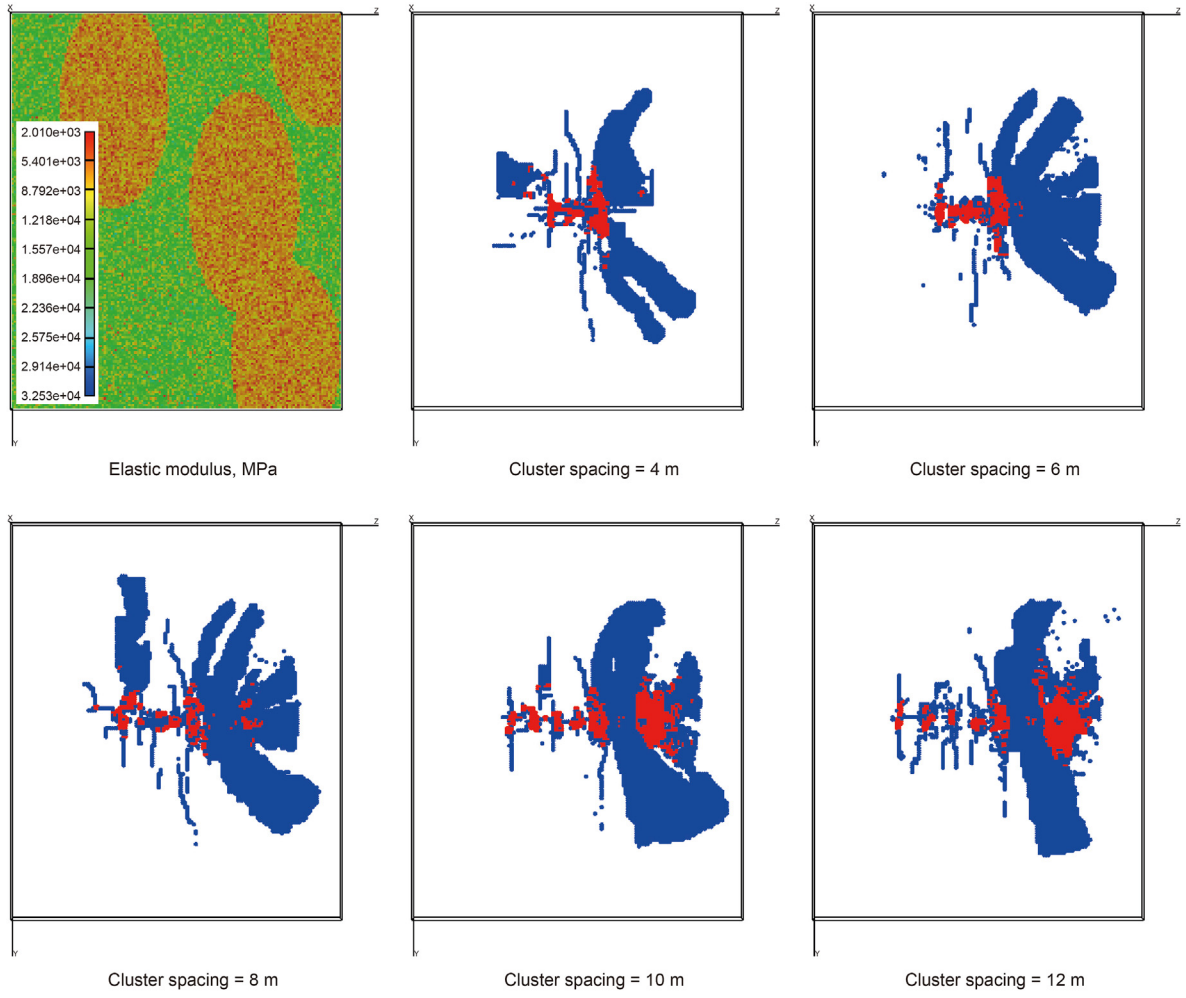

Fig. 12. Simulated acoustic emission of the model slice $x = 9$ m with injected fluids of 2100 m^3, in cases of different cluster spacing (red for shear failure and blue for tensile failure).

variation of the fracture network with the treatment scale was shown in Fig. 16.

Clearly, due to the high clay content, high reservoir rock plasticity, and complex morphology of natural fractures, the fracture propagation is associated with tremendous energy loss, and the SRV in the high-density-bedding reservoir is considerably smaller, compared with those in other types of oil and gas reservoirs. Increasing the fluid volume can greatly promote the SRV. Therefore, the fracturing treatment of the Gulong shale shall moderately increase the fluid injection intensity. However, with the increase of injected fluids, the expansion of the SRV gradually slows down. Hence, a reasonable injected fluid volume (>1500 m^3) is important to ensure the cost-effective recovery of the Gulong shale oil.

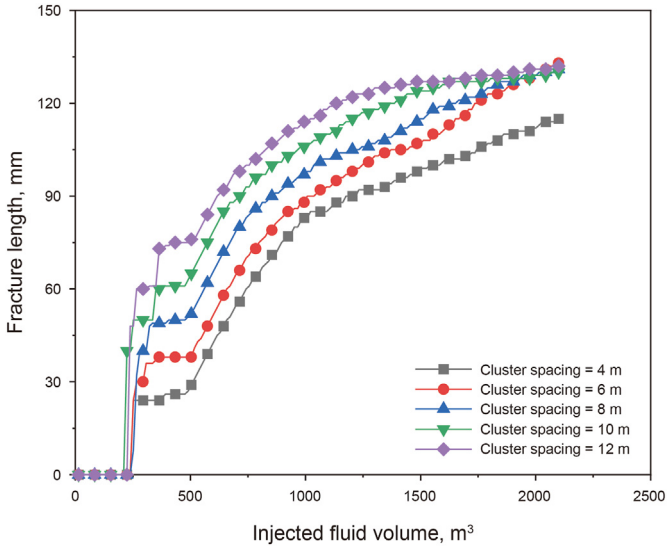

Fig. 13. Influence of cluster spacing on the fracture length.

(5) Influences of fracturing fluid viscosity

The fracturing fluid viscosity is also an important engineering factor affecting the fracturing performance (Li et al., 2022). In fracturing treatments, low-viscosity fracturing fluids can enhance fracture complexity, while high-viscosity fluids help to build high-flow-conductivity channels. To clarify the affecting mechanism of fracturing fluid viscosity on the fracturing performance of the Gulong shale and optimize the fracturing fluid viscosity, a group of simulations with different fracturing fluid viscosities (5, 10, 20, 40 and 60 cP, respectively) were conducted. In these simulations, the bedding quantity was 200, and the cluster spacing is 10 m.

The variation of the maximum average fracture width with fluid viscosity for each simulation is plotted in Fig. 17(a). As the fluid viscosity increases from 5 to 60 cP, the fracture width expands from 8.362 to 14.593 mm. On an overall basis, fracture width is positively correlated with fracturing fluid viscosity. This is mainly because the inferior flow ability of viscous fracturing fluids slows down the dissipation of water pressure in hydraulic fractures. Under such circumstances, the effectively improved fracture net pressure increases fracture width. Moreover, hydraulic fracture length versus injected fluid volume is plotted for simulations with different fluid viscosities (Fig. 17(b)). It is illustrated that the hydraulic fracture extension is notably inhibited by the high viscosity of fracturing fluids. With the viscosity increasing from 5 to 60 cP, the fracture length associated with fluid injection of 1000 m^3 shortens from 117 to 82 m, which represents a reduction by about 30%. Fig. 18 displays the fracture morphologies perpendicular to the horizontal well in the proximity of the perforation cluster, corresponding to injected fluids of 2000 m^3. It is shown that high-viscosity fracturing fluids can effectively improve the net pressure in fractures, help fractures to vertically penetrate bedding, and thus enlarge main fractures; low-viscosity fracturing fluids can effectively promote bedding opening and improve fracture complexity.

The above analysis indicates that viscous fluids are favorable for bedding penetration of fractures and expansion of fracture widths to significantly expand the vertical simulated range and improve the permeability of fractures. Moreover, the limited fracture height

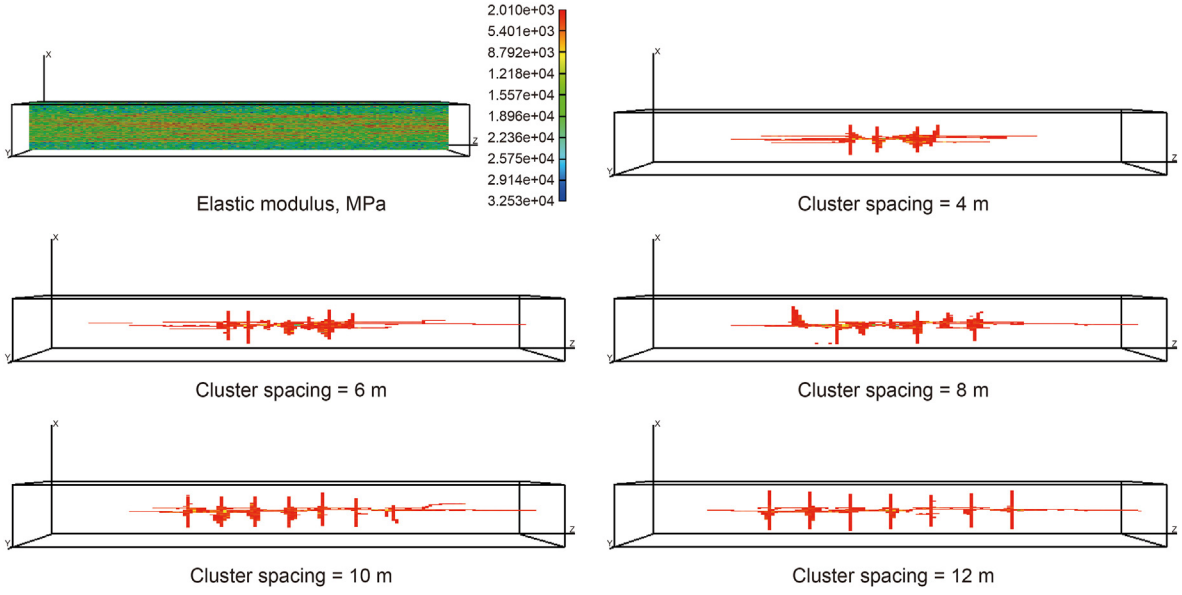

Fig. 14. Fracture networks of the model slice $y = 88$ m with injected fluids of 2100 m^3, in cases of different cluster spacing.

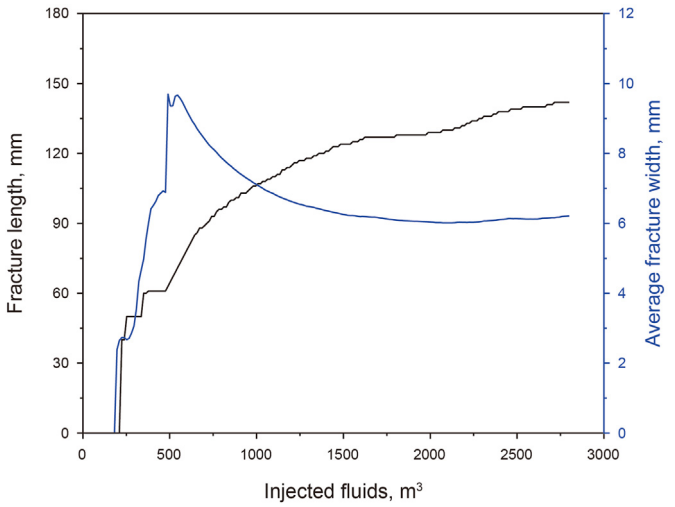

Fig. 15. Fracture length and average fracture width vs. injected fluid volume for the reference case.

is the uppermost constraint for the effective recovery of the Gulong shale oil. Therefore, the fracturing treatment design of the Gulong shale oil shall not blindly follow those of other unconventional reservoirs characterized by large proportions of injected low-viscosity slickwater. Also, it shall be noted that low-viscosity slickwater is beneficial to extending the fracture length, improving fracture complexity, shortening the hydrocarbon migration distance from rock matrix to fractures, and greatly reducing treatment costs. To sum up, it is suggested that the fracturing reservoir stimulation of the Gulong shale reservoir shall adopt the compound fracturing mode to exploit the advantages of both high- and low-viscosity fracturing fluids. Viscous fluids are used to create main fractures and improve the fracture height, and thin fluids are used to activate bedding and extend the fracture length, in order to deliver 3D large-scale reservoir stimulation of the Gulong shale. The viscosity shall be no less than 10 cP.

5. Conclusions

Hydraulic fracturing of shale reservoirs aims at improving fracture complexity and expanding the stimulated reservoir volume (SRV), so as to maximize well productivity. This research targeted the shale of the Qingshankou Formation in the Songliao Basin and clarified the mechanical characteristics of the Gulong shale under the control of multi-scale heterogeneity via the comprehensive refined reservoir characterization and macro-micro-scale mechanical tests. The conclusions are summarized as follows:

(1) Compared with the other reported shale plays in the world, the Gulong shale has high clay mineral content and highly-developed bedding seams, which leads to high plasticity and prominent transverse isotropy of mechanical properties. A three-dimensional (3D) fracture propagation model of hydraulic fracturing was built for the Gulong shale oil with high bedding density, which fully considers the influences of bedding weak planes and in-situ stresses.

(2) The numerical simulation of horizontal well fracturing was performed, based on the actual properties of shale of the 1st Member of the Qingshankou Formation in the Gulong Sag. It was found that the fractures of the Gulong shale present themselves as a main fracture associated with multiple perpendicular branches that have different lengths (resembling the bar-type outdoor directional TV antenna), due to the in-situ stress and high bedding density. The opening of high-density bedding can effectively increase the fracture complexity within the SRV but considerably suppress the fracture height and length. The latter effect combined with the intrinsic high plasticity of the Gulong shale leads to the insufficient horizontal and vertical propagation of artificial fractures, which is the main constraint on the stimulation effectiveness of the Gulong shale oil reservoir.

(3) Numerical simulations showed that bedding density has vital influences on the fracturing stimulation performance, and designs of fracturing parameters shall be adapted to the bedding development of the reservoir. For shale intervals with well-developed bedding, it is suggested to moderately

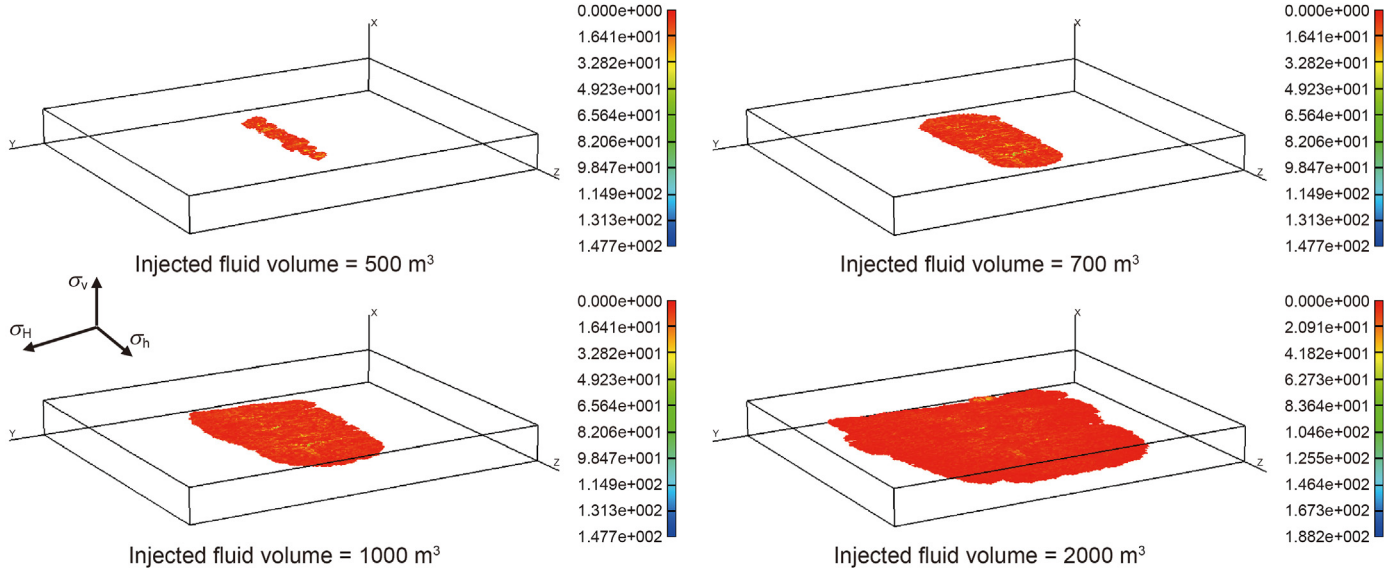

Fig. 16. Fracture width (mm) and fracture morphology of the entire model vs. injected fluid volume.

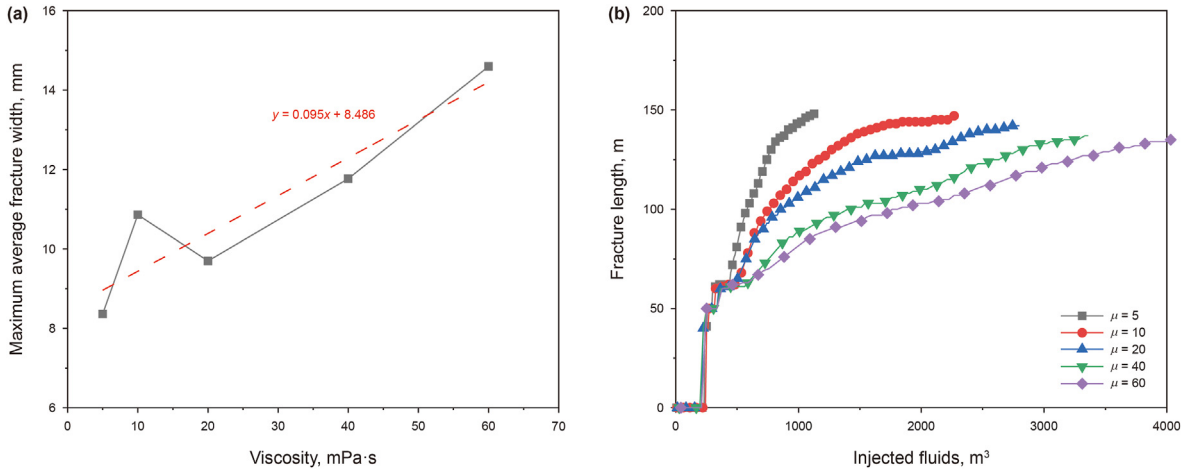

Fig. 17. Influences of fracturing fluid viscosity on the fracture width and length. (**a**) Maximum average fracture width vs. viscosity. (**b**) Fracture length vs. injected fluids, in cases of different viscosities.

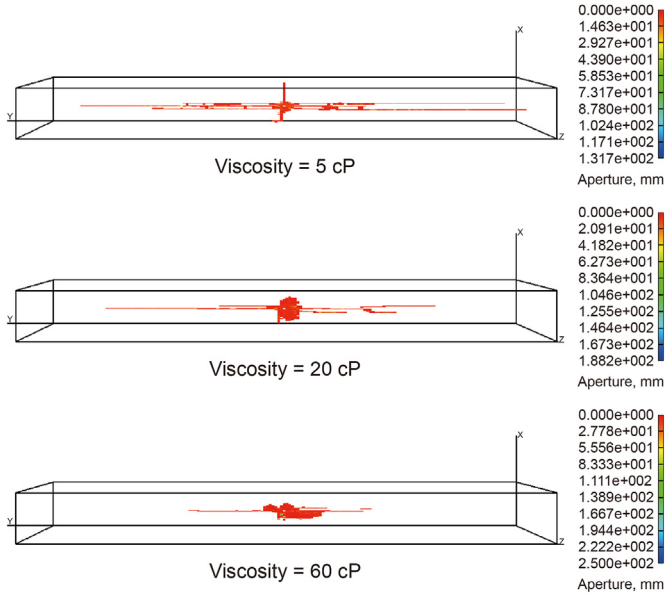

Fig. 18. Fracture networks of the model slice (z = 76 m) with injected fluids of 2000 m^3, in cases of different fluid viscosities.

increase the proportions of high-viscosity fracturing fluids and also the cluster spacing and set a reasonable fluid injection intensity (injected fluid volume), to promote the fracture height, expand the SRV, and improve reservoir stimulation performance of the shale reservoir with high-density bedding. The cluster spacing, viscosity and injected fluid volume shall be greater than 10 m, 10 cP, and 1500 m^3 for Gulong shale reservoir.

Declaration of competing interest

The authors declare that they have no known competing financial interests or personal relationships that could have appeared to influence the work reported in this paper.

Acknowledgements

The research work is supported by the General Program of National Natural Science Foundation of China (No. 52274058), the "Enlisting and Leading" Science and Technology Project of Heilongjiang Province (No. RIPED-2022-JS-1740 and No. RIPED-2022-JS-1853), the Central Program of Basic Science of the National Natural Science Foundation of China (No. 72088101).

References

Chang, X., Shan, Y., Zhang, Z., et al., 2015. Behavior of propagating fracture at bedding interface in layered rocks. Eng. Geol. 197, 33–41. https://doi.org/10.1016/j.enggeo.2015.08.010.

Dong, J., Yuan, G., Wang, X., et al., 2021. Experimental study of multi-timescale crack blunting in hydraulic fracture. Petrol. Sci. 18, 234–244. https://doi.org/10.1007/s12182-020-00479-1.

Feng, Z., Liu, B., Shao, H., et al., 2020. The diagenesis evolution and accumulating performance of the mud shale in Qingshankou Formation in Gulong area, Songliao Basin. Pet. Geol. Oilfield Dev. Daqing 39, 72–85. https://doi.org/10.19597/J.ISSN.1000-3754.202004057 (in Chinese).

Heng, S., Liu, X., Li, X., et al., 2019. Experimental and numerical study on the non-planar propagation of hydraulic fractures in shale. J. Petrol. Sci. Eng. 179, 410–426. https://doi.org/10.1016/j.petrol.2019.04.054.

Jin, X., Li, G., Meng, S., et al., 2021. Microscale comprehensive evaluation of continental shale oil recoverability. Petrol. Explor. Dev. 48, 256–268. https://doi.org/10.1016/S1876-3804(21)60021-6.

Kuang, L., Hou, L., Wu, S., et al., 2022. Organic matter occurrence and pore-forming mechanisms in lacustrine shales in China. Petrol. Sci. 19 (4), 1460–1472. https://doi.org/10.1016/j.petsci.2022.03.005.

Labani, M., Rezaee, R., 2015. The importance of geochemical parameters and shale composition on rock mechanical properties of gas shale reservoirs: a case study from the Kockatea Shale and Carynginia Formation from the Perth Basin, Western Australia. Rock Mech. Rock Eng. 48, 1249–1257. https://doi.org/10.1007/s00603-014-0617-6.

Li, L., Tang, C., Wang, S., et al., 2013. A coupled thermo-hydrologic-mechanical damage model and associated application in a stability analysis on a rock pillar. Tunn. Undergr. Space Technol. 34, 38–53. https://doi.org/10.1016/j.tust.2012.10.003.

Li, N., Yu, J., Wang, D., et al., 2022. Development status of crosslinking agent in high-temperature and pressure fracturing fluid: a review. J. Nat. Gas Sci. Eng. 107, 104369. https://doi.org/10.1016/j.jngse.2021.104369.

Li, T., Li, L., Tang, C., et al., 2019. A coupled hydraulic-mechanical-damage geotechnical model for simulation of fracture propagation in geological media during hydraulic fracturing. J. Petrol. Sci. Eng. 173, 1390–1416. https://doi.org/10.1016/j.petrol.2018.10.104.

Liu, B., Shi, J., Fu, X., et al., 2018. Petrological characteristics and shale oil enrichment of lacustrine fine-grained sedimentary system: a case study of organic-rich shale in first member of Cretaceous Qingshankou Formation in Gulong Sag, Songliao Basin, NE China. Petrol. Explor. Dev. 45, 884–894. https://doi.org/10.1016/S1876-3804(18)30091-0.

Liu, H., Kuang, L., Li, G., et al., 2020. Considerations and suggestions on optimizing completion methods of continental shale oil in China. Acta Pet. Sin. 41, 489–495. https://doi.org/10.7623/syxb202004011 (in Chinese).

Liu, X., Meng, S., Liang, Z., et al., 2023. Microscale crack propagation in shale samples using focused ion beam scanning electron microscopy and three-dimensional numerical modeling. Petrol. Sci. 20 (3), 1488–1512. https://doi.org/10.1016/j.petsci.2022.10.004.

Lu, C., Jiang, H., Yang, J., et al., 2022. Simulation and optimization of hydraulic fracturing in shale reservoirs: a case study in the Permian Lucaogou formation, China. Energy. Rep. 8, 2558–2573. https://doi.org/10.1016/j.egyr.2022.01.189.
Lu, C., Lu, Y., Guo, J., et al., 2020. Stability of the formation interface under the impact of hydraulic fracture propagation in the vicinity of the formation interface. Petrol. Sci. 17, 1101–1118. https://doi.org/10.1007/s12182-019-00416-x.
Meng, S., Li, D., Wang, Q., et al., 2021. Nanoindentation-based three-parameter fracability evaluation method for continental shales. Front. Earth. Sc. 9, 797405. https://doi.org/10.3389/feart.2021.797405.
Nandlal, K., Weijermars, R., 2022. Shale well factory model reviewed: eagle Ford case study. J. Petrol. Sci. Eng. 212, 110158. https://doi.org/10.1016/j.petrol.2022.110158.
Oliver, W., Pharr, G., 1992. An improved technique for determining hardness and elastic modulus using load and displacement sensing indentation experiments. J. Mater. Res. 7, 1564–1583. https://doi.org/10.1557/JMR.1992.1564.
Ouchi, H., Agrawal, S., Foster, J., et al., 2017. Effect of small scale heterogeneity on the growth of hydraulic fractures. In: SPE Hydraulic Fracturing Technology Conference and Exhibition. 24–26 January, the Woodlands, Texas. https://doi.org/10.2118/184873-MS.
Ren, L., Lin, R., Zhao, J., et al., 2018. Stimulated reservoir volume estimation for shale gas fracturing: mechanism and modeling approach. J. Petrol. Sci. Eng. 166, 290–304. https://doi.org/10.1016/j.petrol.2018.03.041.
Sun, L., He, W., Feng, Z., et al., 2022. Shale oil and gas generation process and pore fracture system evolution mechanisms of the continental Gulong Shale, Songliao Basin, China. Energy. Fuels. 36, 6893–6905. https://doi.org/10.1021/acs.energyfuels.2c01407.
Sun, L., Liu, H., He, W., et al., 2021. An analysis of major scientific problems and research paths of Gulong shale oil in Daqing Oilfield, NE China. Petrol. Explor. Dev. 48, 527–540. https://doi.org/10.1016/S1876-3804(21)60043-5.
Veytskin, Y., Tammina, V., Bobko, C., et al., 2017. Micromechanical characterization of shales through nanoindentation and energy dispersive x-ray spectrometry. Geomech. Energy. Envir. 9, 21–35. https://doi.org/10.1016/j.gete.2016.10.004.
Wang, H., Guo, Y., Wang, L., et al., 2017. An experimental study on mechanical anisotropy of shale reservoirs at different depths. Rock Soil Mech. 38, 2496–2506. https://doi.org/10.16285/j.rsm.2017.09.005.
Wang, T., Liu, Z., Gao, Y., et al., 2018. Theoretical and numerical models to predict fracking debonding zone and optimize perforation cluster spacing in layered shale. J. Appl. Mech. 85, 011001. https://doi.org/10.1115/1.4038216.
Wang, Y., Li, X., Zhang, B., et al., 2016. Optimization of multiple hydraulically fractured factors to maximize the stimulated reservoir volume in silty laminated shale formation, Southeastern Ordos Basin, China. J. Pet. Sci. Eng. 145, 370–381. https://doi.org/10.1016/j.petrol.2016.05.033.
Zhang, Y., Wei, X., Tang, P., et al., 2020. Fracture propagating mechanism and fracturing engineering technology in Gulong shale oil reservoirs of Songliao Basin. Pet. Geol. Oilfield Dev. Daqing 39, 170–175. https://doi.org/10.19597/J.ISSN.1000-3754.202004060 (in Chinese).
Zhao, P., Xie, L., Fan, Z., et al., 2021. Mutual interference of layer plane and natural fracture in the failure behavior of shale and the mechanism investigation. Petrol. Sci. 18, 618–640. https://doi.org/10.1007/s12182-020-00510-5.
Zhao, W., Hu, S., Hou, L., et al., 2020. Types and resource potential of continental shale oil in China and its boundary with tight oil. Petrol. Explor. Dev. 47 (1), 1–11. https://doi.org/10.1016/S1876-3804(20)60001-5.
Zhao, X., Jin, F., Liu, X., et al., 2022. Numerical study of fracture dynamics in different shale fabric facies by integrating machine learning and 3-D lattice method: a case from Cangdong Sag, Bohai Bay basin, China. J. Petrol. Sci. Eng. 218, 110861. https://doi.org/10.1016/j.petrol.2022.110861.
Zhou, T., Wang, H., Li, F., et al., 2020. Numerical simulation of hydraulic fracture propagation in laminated shale reservoirs. Petrol. Explor. Dev. 47, 1117–1130. https://doi.org/10.1016/S1876-3804(20)60122-7.
Zou, C., Dong, D., Wang, Y., et al., 2016. Shale gas in China: characteristics, challenges and prospects (II). Petrol. Explor. Dev. 43, 182–196. https://doi.org/10.1016/S1876-3804(16)30022-2.